atmosphere

MDPI

Article

First Major Eruption of Solar Cycle 25: Impacts of the 3 July 2021 X1.59 Solar Flare on the Ionosphere and Primary Cosmic Rays

Vladimir A. Srećković, Nikola Veselinović, Aleksandra Kolarski *, Mihailo Savić, Žarko Medić, Milica Langović, Filip Arnaut

Institute of Physics Belgrade, University of Belgrade, P.O. Box 57, 11001 Belgrade, Serbia; vlada@ipb.ac.rs (V.A.S.); veselinovic@ipb.ac.rs (N.V.); msavic@ipb.ac.rs (M.S.); zarko.medic@ipb.ac.rs (Ž.M.); langovic@ipb.ac.rs (M.L.); arnaut@ipb.ac.rs (F.A.)

* Correspondence: aleksandra.kolarski@ipb.ac.rs; Tel.: +381-11-37-13-000

Abstract

The X1.59 solar flare on 3 July 2021, was the first X-class flare of Solar Cycle 25 and the first since the X-class flare on 10 September 2017. This event was notable for producing a rare geomagnetic crochet, a temporary and localized perturbation in Earth's magnetic field during the flare's peak. To the best of our knowledge, this study represents the first VLF-based analysis of this event, as well as the first comprehensive multi-instrument investigation of it. VLF observations from the NAA and DHO transmitters were used to investigate the ionospheric response via amplitude and phase variations. Key low ionosphere parameters, including the effective reflection height, sharpness factor, time delay and electron density profiles were derived. The results reveal rapid ionospheric responses closely correlated with X-ray flux peaks, including sudden phase and amplitude perturbations indicative of increased low ionosphere ionization and the geomagnetic crochet effect. Simultaneously, cosmic-ray measurements from ground detectors showed negligible modulation and no significant Forbush decrease, consistent with the flare's weak and partially Earth-directed CME. Also, the spectrum of energetic protons measured in-situ in near-Earth space shows little disturbance. This integrated study demonstrates the sensitivity of the lower ionosphere to intense solar radiation and highlights the limited short-term impact on cosmic-ray and solar energetic proton flux, providing a comprehensive assessment of flare-driven space-weather effects during the early phase of Solar Cycle 25.

Keywords: solar flares; solar cycle 25; atmospheric ionization; sudden ionospheric disturbances; ionospheric parameters; neutron monitor; muon detector; solar energetic particles; cosmic ray flux; extreme radiation

Academic Editor: Masashi Hayakawa

Received: 30 December 2025
Revised: 7 February 2026
Accepted: 8 February 2026
Published: 10 February 2026

1. Introduction

Solar wind plays a fundamental role in shaping the heliosphere and mediating the interaction between solar activity and planetary environments. It is a continuous, supersonic outflow of plasma from the solar corona, composed primarily of electrons, protons, and alpha particles, with embedded interplanetary magnetic fields carried outward from the Sun. Superimposed on quasi-steady solar wind, transient solar events can produce significant enhancements in the flux and energy of charged particles [1]. Among these events, X-class flares, resulting from the rapid release of stored magnetic energy through magnetic reconnection in active regions, can lead to intense electromagnetic radiation across the spectrum and efficient acceleration of charged particles. Following X-class flares, an additional

flux of high energy charged particles, commonly referred to as solar energetic particles or SEPs, is frequently observed. These particles, predominantly protons but also including electrons and heavier ions, can be accelerated to relativistic energies either directly at flare reconnection sites or at shock fronts when the flare is accompanied by a coronal mass ejection. The resulting SEP events produce pronounced, time-dependent enhancements in particle fluxes that propagate through the heliosphere along interplanetary magnetic field lines, often reaching Earth within minutes to hours after flare onset. The injection of this additional charged particle population significantly alters the local plasma environment and enhances geomagnetic activity through interactions with planetary magnetospheres.

Solar flares (SFs) and coronal mass ejections (CMEs) have long been recognized as the main drivers of space-weather disturbances that affect the ionosphere [2–4].

It is well established that CME is a large-scale eruption of hot, magnetized plasma that is often closely associated with a solar flare. Unlike flare radiation, which reaches Earth in minutes, the charged particles carried by a CME require one to several days to arrive. Upon impact, the CME's magnetic field and energetic particles can cause further disturbances to radio communication, satellite operations, and electrical power systems (e.g., [5–7]). These eruptions modify ionization in the upper atmosphere, where enhanced X-ray and EUV radiation and CME-driven disturbances alter ionospheric conditions and impact radio-wave propagation [8–12]. The resulting ionization changes depend on flare class and temporal evolution [13,14], and are commonly diagnosed using Very Low Frequency (VLF)–Low Frequency (LF) radio techniques [15–24]. These disturbances can disrupt GNSS and HF communication and may induce short-lived magnetic responses such as geomagnetic crochets [25–28]. Near solar-cycle maximum, SFs are often followed by CMEs [29], whose interplanetary counterparts (ICMEs) transport plasma and magnetic flux, accelerate SEPs and local Energetic Storm Particle (ESPs), and are continuously monitored by spacecraft [30]. ICME-driven IMF enhancements modulate galactic cosmic rays, producing Forbush decreases (FDs) characterized by rapid CR depressions and gradual recoveries [31], with well-established links to solar-wind parameters [32–34]. Because extreme space-weather events pose risks to satellites, communications, aviation, and human spaceflight, despite their relatively low but non-negligible occurrence probability [35], understanding ionospheric responses to SFs remains crucial for technological resilience and forecasting capability [36–39].

Connection between SEP and the impact of the X1.59 Solar Flare of 3 July 2021 on CR flux and heliospheric and ionospheric disturbance can lead to better understanding of complex phenomena that starts at the Sun and end on Earth surface.

The X1.59 flare on 3 July 2021 was the first X-class solar flare of Solar Cycle 25 and the first since the X-class flare on 10 September 2017. The X1.59 solar flare of 3 July 2021 began at 14:18 UT, reached its peak intensity at 14:29 UT, and concluded at 14:34 UT, with a time duration of approximately 16 min, characterized as a short-duration SF. This flare was notable for causing a rare phenomenon called a geomagnetic crochet, which involves a temporary, localized change in Earth's magnetic field during the flare's peak.

The X1.59 (X1.5) SF originated from Active Region AR 2838 (see Figure 1a), positioned near the solar limb. The flare peaked at 14:29 UTC and was detected by the GOES-16 satellite as a sudden, intense burst of X-ray radiation (Figure 1b). This eruption produced a strong R3 (Strong) radio blackout on Earth's sunlit hemisphere and triggered a rare geomagnetic crochet—a brief, simultaneous disturbance in Earth's magnetic field caused by enhanced ionospheric currents induced by the flare's intense X-ray and extreme ultraviolet (EUV) emissions. Unlike typical geomagnetic storms that occur hours or days after CMEs, the crochet occurred almost instantaneously during the flare's peak [40–43]. Although the associated CME was weak and only partially Earth-directed [44], leading to minimal geomagnetic activity and no significant Forbush decrease in cosmic-ray intensity, the event provided valuable insight

into solar–terrestrial coupling processes. The X1.59 flare can show that even in the early stages of Solar Cycle 25, the Sun was capable of producing high-energy, geoeffective events, signaling the increasing solar activity expected in the coming years.

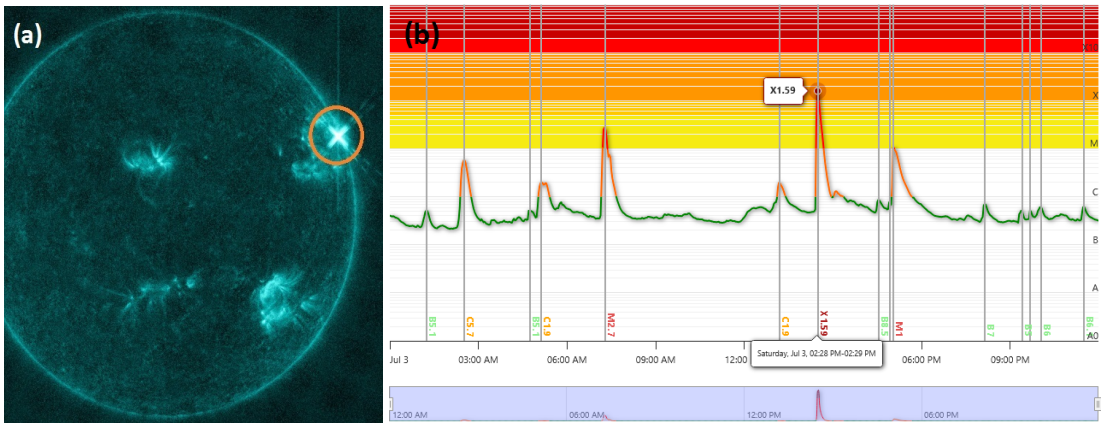

Figure 1. Solar flare impacts observed on 3 July 2021: (**a**) the position of active region AR 2838 (shown by the orange round marker) on the solar disk; and (**b**) the solar flares detected, with yellow to red shading representing increasing intensity of X-class flares.

The ionospheric response to the 3 July 2021 X1.59 solar flare was immediate and pronounced, producing a strong dayside enhancement in ionization and a rare geomagnetic crochet. The sudden increase in X-ray and EUV radiation rapidly intensified ionization in the E-region, strengthening ionospheric current systems, particularly the solar quiet (Sq) current. This led to a short-lived but clearly detectable deflection in ground-level magnetic field measurements at several dayside observatories, characteristic of a crochet-type disturbance. This effect, occurring within minutes of the flare peak, distinguished the event from the delayed geomagnetic perturbations typically associated with CME-driven storms. Although the accompanying CME was weak and only marginally Earth-directed, resulting in minimal long-term geomagnetic activity, the flare itself generated a notable R3-class radio blackout and significant signal absorption in the D- and E-regions of the ionosphere. Overall, the event highlighted the sensitivity of the dayside ionosphere and geomagnetic field to impulsive high-energy solar radiation, independent of subsequent solar-wind-driven disturbances.

During major solar events, disturbances are clearly evident in SEP fluxes as sharp intensity enhancements, often showing velocity dispersion (higher-energy particles arriving first) that can be followed by prolonged elevations due to CME-driven shocks. Such signatures are prominently visible in multi-channel proton flux time series, where lower-energy channels exhibit delayed onsets and higher peak intensities compared to higher-energy channels. These data not only confirm the solar origin of the particles but also help characterize the acceleration mechanisms and interplanetary transport conditions during the event. There are two possible processes leading to SEP acceleration [45]. The first is related to type II radio bursts from coronal and interplanetary shock waves. The second process is associated with type III radio bursts which are produced by streaming electrons. The former is driven by fast CMEs, is proton-dominated, and produces "gradual" SEP events—which can last for days, partly due to the continuing acceleration of the shock—that have high SEP flux intensity near Earth.

The latter mechanism is predominantly connected to magnetic reconnection with open magnetic field lines and wave–particle interactions in SFs and jets. The relatively short duration and the rather low magnitude of the SEP enhancement potentially associated with the X1.59 solar flare on 3 July 2021 is more consistent with the second type.

Simultaneously, cosmic ray ground measurements from worldwide neutron and muon detector networks showed negligible modulation of cosmic rays and no significant

Forbush decrease, consistent with the flare's weak and partially Earth-directed CME and the impulsive SEP event associated with the flare.

To the best of our knowledge, this work constitutes the first VLF-based analysis of the low-ionospheric response to this event, as well as the first comprehensive multi-instrument investigation of it. In addition, complementary Total Electron Content (TEC) measurements were employed to evaluate the ionospheric disturbances at higher altitudes, providing the only available space-weather diagnostics in the absence of dedicated D-region instrumentation or direct measurements. For additional information and detailed analyses related to this event, the reader is referred to a range of complementary studies and reports, including recent scientific investigations and space-weather bulletins [46–53].

The processes that usually occur during major eruptions on the Sun are characterized by:

- The CME (with its magnetic cloud and sheath) travels through interplanetary space, disturbs the interplanetary magnetic field, and acts as a barrier to galactic cosmic rays.
- This suppression of cosmic-ray influx leads to a noticeable drop in cosmic-ray intensity at the Earth, known as a Forbush decrease.
- Enhanced X-ray and EUV radiation from the flare produces rapid ionization in the lower ionosphere (especially the D-region), modifying electron densities, conductivity, and the propagation of VLF radio waves.
- During the flare's impulsive phase, sudden increases in ionospheric currents may induce a short-lived geomagnetic perturbation at the Earth's surface, known as a geomagnetic crochet.

Figure 2 provides a schematic overview linking the 3 July 2021 solar flare and associated CME to both effects on cosmic rays and the lower-ionospheric (VLF) response. The shock–sheath region and the magnetic cloud of a CME act as transient magnetic barriers that modulate the flux of galactic cosmic rays, producing a Forbush decrease that can be detected on Earth's surface. At the same time, flare-driven X-ray/EUV radiation and energetic particles enhance D-region ionization, leading to measurable perturbations in VLF amplitude and phase along subionospheric paths.

The structure of the paper is as follows: Section 2 outlines the monitoring methods and the modeling approach used to derive outputs; Section 3 presents the results together with their interpretation; and Section 4 summarizes the discussion, main conclusions and future research.

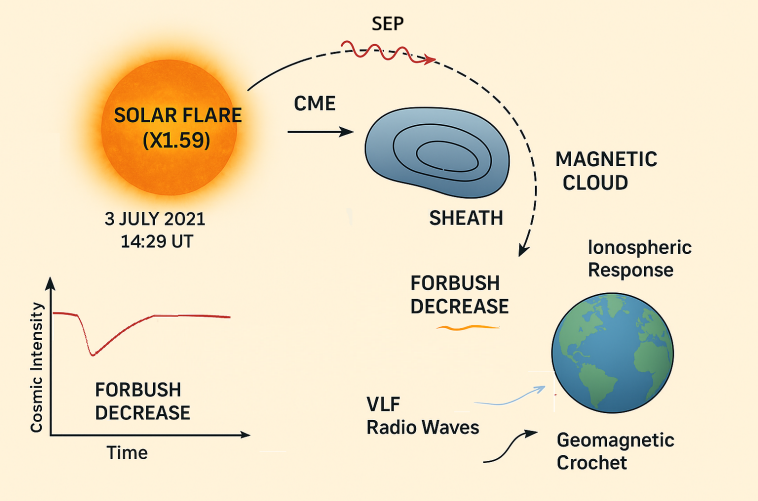

Figure 2. Schematic linking a solar flare/CME to a Forbush decrease and lower-ionospheric (VLF) effects. The CME shock/sheath and magnetic cloud modulate galactic cosmic rays, producing a Forbush decrease at the Earth, while flare radiation and energetic particles ionize the D-region, altering VLF propagation.

2. Materials and Methods

For this multi-instrument data study, various types of data were necessary that include, among others, heliospheric data measured near Earth, at Lagrange point L1, outside the geomagnetic field, other energetic proton data measured near Earth like selected energetic proton data, the interplanetary magnetic field (IMF), CME, solar wind, and geomagnetic field parameters. The comprehensive repository focused on acquiring these data, mostly in the form of time series, was the OMNIWeb Plus repository provided by the NASA/Goddard Space Flight Center [54]. Minute data for energetic proton data from this repository were provided by the Energetic and Relativistic Nuclei and Electron (ERNE) sensor unit onboard the Solar and Heliospheric Observatory (SOHO) [55]. SOHO/ERNE is composed of two energetic particle sensors: the Low-Energy Detector (LED) and the High-Energy Detector (HED), each with ten energy channels measuring ion fluxes and count rates in the ranges of 1.3–13 MeV/nucleon and 13–130 MeV/nucleon, respectively. [56]. IMF and solar wind speed data in the OMNIWeb Plus repository were provided by the Global Geospace Science (GGS) WIND spacecraft [57].

In this study, for the period of interest, we utilized in-situ measurements obtained by the Solar and Heliospheric Observatory (SOHO) and the Wind spacecraft near the Sun–Earth Lagrange point L1. Spatial components of interplanetary magnetic field and solar wind plasma parameters such as energetic proton speed, density, and temperature were obtained from the time-shifted, bow-shock-nose-propagated OMNI database, which incorporate mainly data from the Wind spacecraft. Proton flux data at L1 were taken from the Energetic and Relativistic Nuclei and Electron (ERNE) instrument aboard SOHO in hourly-resolution.

When establishing a potential source of SEP enhancements, it is important not only to identify a candidate source but also to eliminate alternative ones. To this end, we consulted a number of online repositories covering different phenomena, including the SOHO/LASCO CME catalog [44,58] for coronal mass ejections, the Richardson–Cane catalog [59] for interplanetary CMEs, and compilations of ground-level enhancements and large proton intensifications, including those produced by the ERNE team and cross-referenced with reports from the NOAA Space Weather Prediction Center.

At the IPB, Serbia, a high-sensitivity VLF system is operated as a key element of the Belgrade sudden ionospheric disturbance monitoring network. The instrumentation consists of narrowband VLF receivers optimized for continuous monitoring of subionospheric signal propagation on selected transmitter frequencies [60,61]. These receivers employ stable, low-noise front-end amplifiers and precisely tuned filters, enabling the detection of small amplitude and phase fluctuations caused by D- and lower E-region electron density variations. Signals from powerful VLF transmitters, such as those in Europe (e.g., DHO, GQD, GBZ) or worldwide (NAA, NWC, etc.), are recorded with high temporal resolution, typically 20 Hz or better, allowing the system to capture rapid ionospheric changes produced by solar flares, lightning discharges, and other geophysical disturbances. Data are digitized and logged continuously, then processed using specialized software for spectral, wavelet, and time-series analysis. The Belgrade group's long-term VLF records have become an important resource for studying flare-induced ionospheric perturbations, including sudden phase anomalies, amplitude jumps, and modal interference patterns, making this instrumentation a valuable component of international sudden ionospheric disturbance (SID) and VLF research collaborations (see e.g., papers [62–66]).

In this research, VLF measurements were obtained using the narrowband receiver system operated by the IPB, which continuously records the amplitude and phase of selected subionospheric VLF transmitter signals with high temporal resolution ($\geq$20 Hz). Raw data were preprocessed to remove instrumental offsets and high-frequency noise,

after which amplitude $A(t)$ and phase $P(t)$ perturbations associated with the solar flare were extracted; see e.g., [60,67]. The correlated solar X-ray fluxes obtained from the GOES-16 satellite were examined simultaneously with the analysis of VLF data. The GOES-16 satellite used X-ray sensors in the 0.1–0.8 nm range to measure the strength of X-ray irradiance [53].

The important ionospheric parameter, i.e., time delay Δt, is defined as the difference between the moment when the VLF amplitude reaches its maximum ($t_{A\max}$) and the time of peak X-ray irradiance ($t_{I\max}$) [60]. This delay is closely related to the characteristic "sluggishness" of the lower ionosphere response to solar flare-induced ionization [68] and represents a valuable parameter for studying ionospheric reactions to solar flares [13,69]. It provides valuable insight into D-region dynamics, energy deposition efficiency, quantifying recombination rates, and flare–ionosphere coupling mechanisms, and is widely used for validating ionospheric models and improving space-weather predictive capabilities. The value of Δt depends on the flare intensity and other environmental conditions, and typically falls within a range of a few minutes [70]. According to a paper by Srećković et al. [70] and Hayes et al. [71], one can see that Δt data are scattered, with up to 10 min and with a mean value of about two–three minutes.

To quantify the corresponding changes in the lower ionosphere, the two-parameter model was applied, using the effective reflection height h' and sharpness factor β to describe lower ionosphere conductivity profiles. For details, see, e.g., [66,72,73]. Their accurate determination enables better diagnostics and prediction of space weather impacts on communication systems. The corresponding electron density profiles were calculated using the standard EasyFit method [61] and FlarED method [70]. This procedure provides a quantitative reconstruction of lower ionosphere electron density evolution during the flare-driven ionospheric disturbance.

3. Results and Discussion

The X1.59 solar flare of 3 July 2021 was the first X-class flare of Solar Cycle 25 and the first such event since the X-class flare of 10 September 2017. The flare commenced at 14:18 UT, reached its peak intensity at 14:29 UT, and ended at 14:34 UT. This event was notable for producing a rare geomagnetic crochet, characterized by a temporary and localized deflection of Earth's magnetic field during the flare's peak phase. The intense pulse of soft X-ray radiation significantly enhanced ionization in the lower ionosphere, leading to a shortwave radio blackout reported by the space weather observatory in Norway and anomalous radio propagation at frequencies below 30 MHz. The flare also generated a radio burst, triggered sudden ionospheric disturbances, and induced enhanced current systems extending from approximately 60 km to between 100 and 600 km above Earth's surface, capable of modifying the polar magnetic field and producing detectable ground-level magnetic perturbations. Owing to the short-duration yet intense ionization enhancement, this event is particularly well suited for VLF diagnostics and multi-instrument analysis. Although the flare produced a strong ionospheric response, it produced recognizable yet minor heliospheric disturbance observable in the heliospheric parameters detected via detectors onboard space probes at L1. It has no influence on CRs because the disturbance created in the heliosphere with the passing of additional particles most likely originated from the active region, and was too weak to produce modulation on CRs with an energy of more then 1 GeV that can be detected on Earth with ground detectors.

3.1. Ionosphere

In order to better understand the processes driving ionospheric changes during the X1.59 solar flare of 3 July 2021, variations in solar X-ray radiation flux were examined. These observations were provided by the X-Ray Irradiance Sensor (XRS) carried by the GOES-R (Geostationary Operational Environmental Satellite–R Series) satellite [53]. The 3 July 2021 X1.59 solar flare produced strong and immediate disturbances in VLF propagation and high-frequency (HF) radio communication across the sunlit hemisphere. The sudden enhancement of X-ray and EUV radiation caused rapid ionization in the D- and lower E-regions, sharply increasing electron densities and leading to significant VLF phase and amplitude perturbations recorded by ground-based receivers. These SIDs included abrupt phase advances, signal absorption, and mode conversion effects along VLF paths. At higher radio frequencies, the flare triggered an NOAA-classified R3 Strong radio blackout over the Atlantic Ocean, reducing HF communication reliability and causing partial signal loss in aviation and maritime systems operating on the dayside. VLF instruments, including narrowband receivers in northern Europe and the USA, clearly captured the onset of the flare as a characteristic step-like change consistent with rapid D-region modification. Overall, the event demonstrated the strong sensitivity of Earth's lower ionosphere to intense solar radiation, with VLF and HF observations providing precise timing markers for the flare's radiative impact.

The correlated solar X-ray 0.1–0.8 nm flux, obtained from the GOES-16 satellite, were examined simultaneously with the analysis of VLF data. The GOES spacecraft monitor solar X-ray emission in two spectral bands: the 0.1–0.8 nm range, commonly designated as the long (XL) channel, and the 0.05–0.4 nm range, referred to as the short (XS) channel [53]. For the purposes of this study, the primary parameter of interest is the X-ray flux intensity in the 0.1–0.8 nm band, as it is most directly related to the ionospheric response observed in the VLF measurements.

Numerical simulations conducted in this paper rely on application of the FlarED' method and an approximate analytic expression application called EasyFit. The methodology used relies on the simultaneous monitoring of several VLF signals during regular and irregular ionospheric conditions, both for amplitude and phase.

In Figure 3, the 24-h behavior of subionospheric VLF amplitudes reveals the ionospheric response to the X1.59 solar flare of 3 July 2021. Panel (a) shows the amplitude of the NAA transmitter signal emitted from the USA towards Belgrade, while panel (b) presents the amplitude of the DHO transmitter signal emitted from Germany towards Belgrade. These stations, i.e., transmitters, were affected by the event. The figure highlights how both signals responded to the enhanced solar X-ray extreme radiation throughout the day, with rapid increases corresponding to the flare's peak intensity. These amplitude variations provide insight into the changing electron density and conductivity of the lower ionosphere, demonstrating the sensitivity of long-distance VLF propagation to solar radiation. By comparing the NAA and DHO signals, differences in response due to a relatively long propagation path, with a GCP-NAA of approximately 6.6 Mm and a short GCP-DHO of approximately 1.3 Mm, respectively, transmitter frequency and local ionospheric conditions can be observed, offering a comprehensive view of the lower ionospheric dynamics during the solar flare event.

Figure 4 shows the simultaneous variations in X-ray flux and VLF signal characteristics observed during the most turbulent interval (14:00–18:00 UT) on 3 July 2021. Specifically, panels (a) through (e) display the GOES-16-measured X-ray flux in soft-range, the DHO phase signal, the NAA phase signal, and the DHO and NAA amplitude signals, respectively. The figure highlights the rapid response of the lower ionosphere to the X1.59 solar flare,

with clear correlations between the X-ray flux peaks and abrupt changes in both phase and amplitude of the VLF signals.

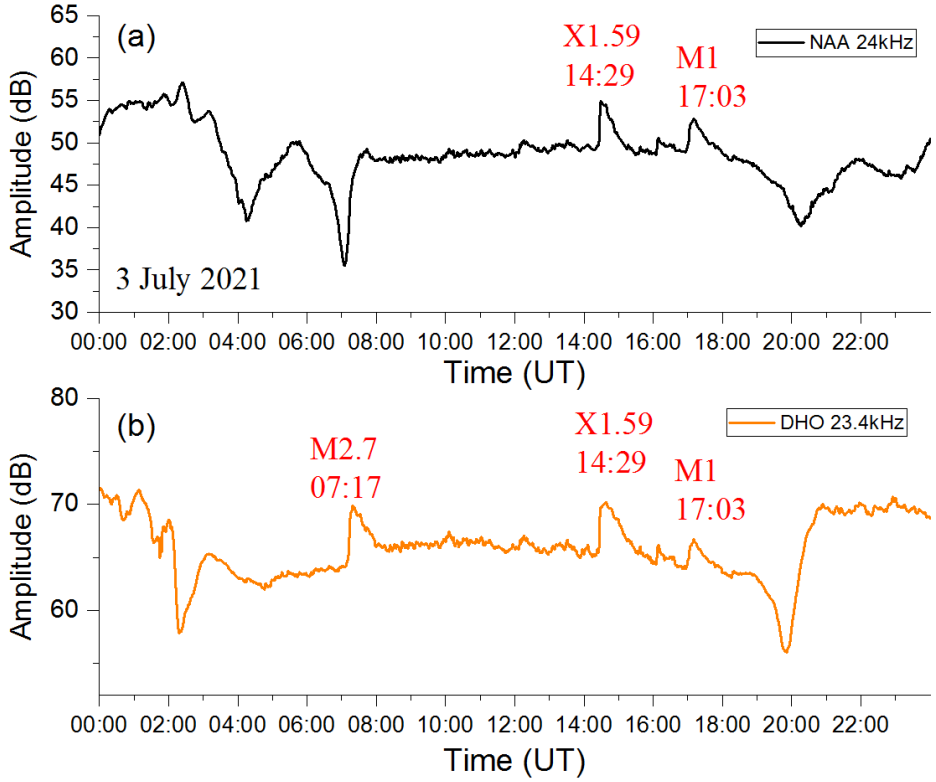

Figure 3. Ionospheric response to the SFs, represented by 24 h variations in the NAA (**a**) and DHO (**b**) VLF signal amplitudes observed on 3 July 2021 recorded in Belgrade.

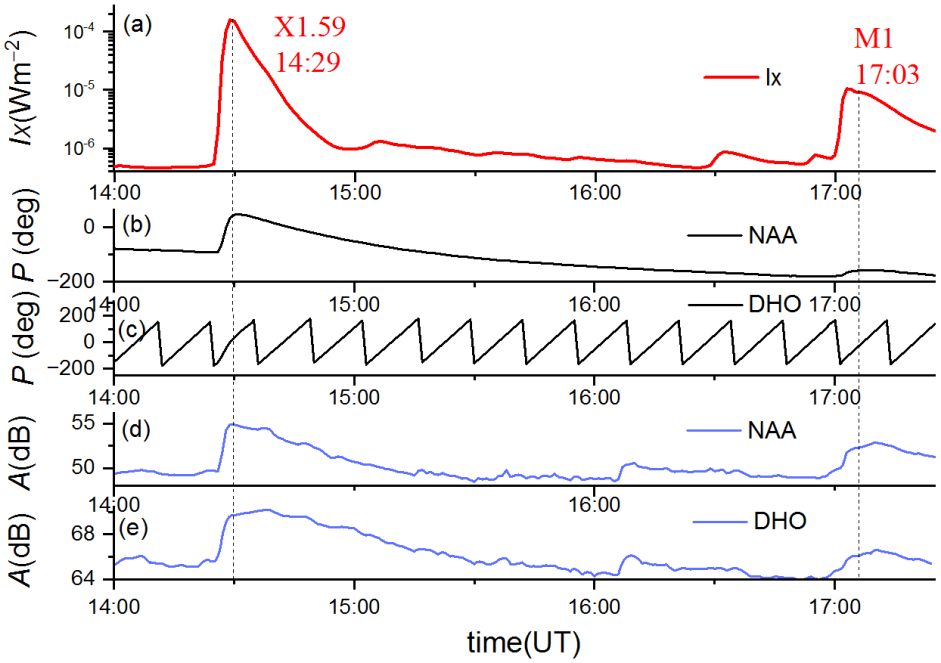

Figure 4. variations in X-ray flux from the GOES-16 satellite, soft-range, DHO, NAA phase signal recorded in Belgrade, and DHO, NAA amplitude signal recorded in Belgrade (**a**–**e**), respectively, during the most turbulent interval (14:00–18:00 UT) on 3 July 2021.

The NAA amplitude jumped as expected for that class of flares ($\Delta A = 6$ dB), and on the other hand, the phase jumped a little more than expected (ΔP, reaching more than a

hundred degrees). This was probably due to the presence of a magnetic crochet, probably because GCP (NAA—Belgrade) was whole and, i.e., exposed longer to the magnetic crochet than DHO—Belgrade. So, the signal experienced a major change. No noticeable change is observed in the DHO phase signal, although the amplitude signal shows a noticeable change ($\Delta A = 5$ dB). Phase perturbations reflect modifications in the effective reflection height and electron density of the D-region, while amplitude variations indicate changes in ionospheric conductivity and propagation conditions along the subionospheric paths. By simultaneously presenting these parameters, the figure provides a comprehensive view of the flare-induced ionospheric disturbances and demonstrates the sensitivity of VLF signals to rapid solar radiation enhancements during the flare's peak activity.

According to [70], the important parameter time delay between the peak X-ray flux and the corresponding maximum in VLF amplitude, Δt, is typically around 3 min on average. Using the empirical relation from [70], $\Delta t = a + b\log(I_x)$, the estimated time delay for the X1.59 flare is approximately 2 min. In the present analysis, the time delay Δt is found to be notably short, with a measured value of roughly 60 s—approximately half of the theoretically estimated value. This is probably due to the specificity of the case where the crochet effect appears.

In Figure 5, the simultaneous changes in major ionospheric quantities and the corresponding X-ray flux in soft-range during the 3 July 2021 X1.59 flare are displayed. Panels (a) through (e) show, respectively, the effective reflection height h', the sharpness parameter β, the electron density at reference height ($h = 74$ km) derived from the flare-induced model $N_{e,\mathrm{FlarED}}$ [61], the electron density obtained using the EasyFit procedure $N_{e,\mathrm{EasyFit}}$ [70], and the GOES-16-measured X-ray flux in soft-range [53]. The figure highlights the rapid response of the lower ionosphere to enhanced solar radiation, with clear correlations between the flare's X-ray peak and changes in h', β, and the electron density profiles. The comparison between $N_{e,\mathrm{FlarED}}$ and $N_{e,\mathrm{EasyFit}}$ demonstrates the consistency of two independent modeling approaches, while the temporal alignment with the X-ray flux provides a direct link between solar forcing and D-region ionization dynamics.

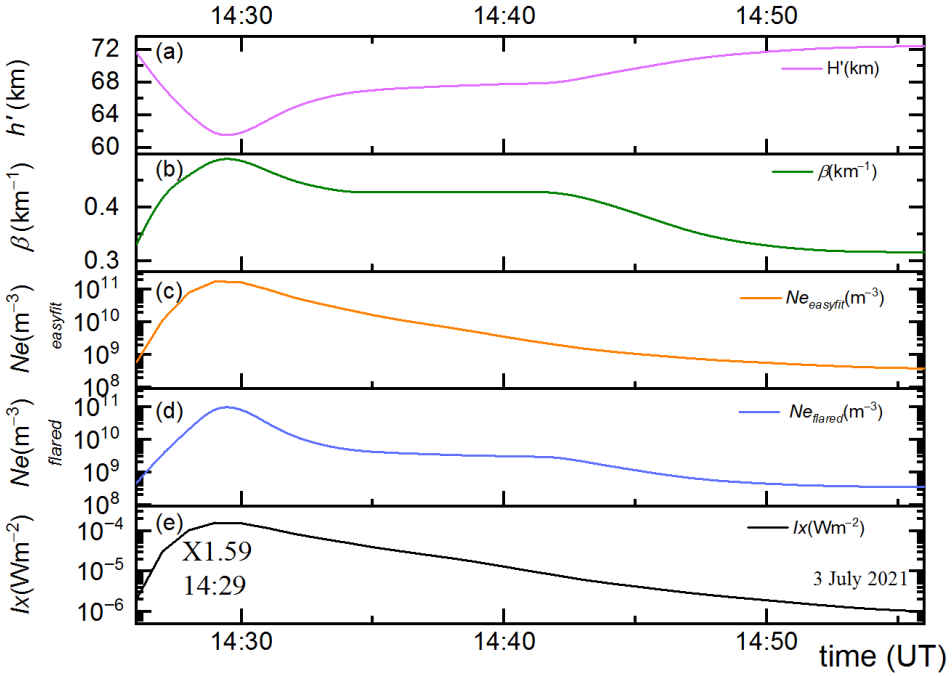

Figure 5. Simultaneous variations of the effective reflection height h', sharpness β, Ne_{FlarED}, $Ne_{EasyFit}$ at reference height and X-ray flux from GOES-16, soft-range, from (**a**–**e**), respectively, during the X1.59 X-ray flares of 3 July 2021.

The evolution of the solar X-ray flux 0.1–0.8 nm recorded by the GOES-16 satellite (Figure 6a) and the corresponding altitude profile of the electron density N_e (m^{-3}) during the X1.59 solar flare (Figure 6b) are depicted in Figure 6. It can be observed that the electron density increases with increasing altitude and that it experiences a maximum during the peak of a solar flare. The electron density increased by almost a few orders of magnitude during the case of SF events and altitude changes. The data are important for the characterization and modeling of the lower ionosphere under extreme conditions. This combined view allows a comprehensive assessment of the flare-driven ionospheric perturbations over the event's duration. Moreover, a geomagnetic crochet represents a uniquely rapid Sun-to-Earth coupling effect, linking flare radiation, ionospheric current enhancement, and observable VLF disturbances.

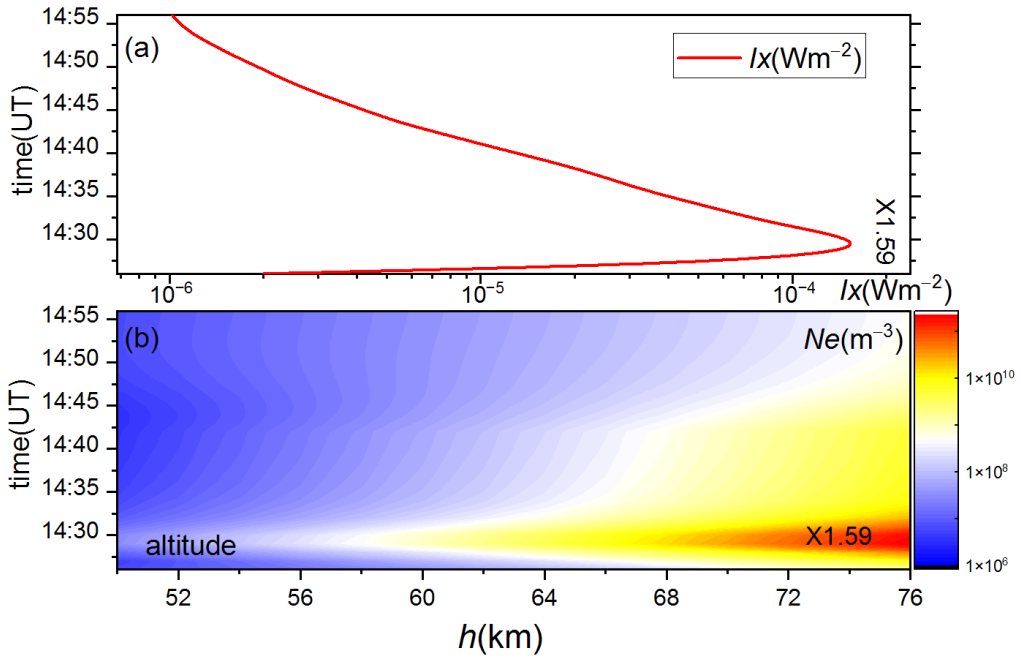

Figure 6. (**a**): The X-ray flux in the soft spectral range (XL, 0.1–0.8 nm), recorded by the GOES-16 satellite; (**b**): the corresponding altitude-dependent electron density distribution during the X1.59 solar flare of 3 July 2021. The profiles were derived using the FlarED approach.

Using Equation (11) from [68], the effective electron recombination coefficient α can be related to the observed ionospheric response time through

$$\alpha = \frac{1}{2\, N_e(I_{\max})\, \Delta t}$$

which provides a practical expression for evaluating α from VLF and X-ray observations. For the X1.59 flare analyzed in this study, the resulting value for the effective electron recombination coefficient α at the reference height is $\alpha \approx 1 \times 10^{-11}$ $m^3 s^{-1}$, which is fully consistent with established D-region ionospheric chemistry. Typical values reported in the literature span 10^{-12} to 10^{-10} $m^3 s^{-1}$, depending on altitude, background ionization, and dominant ion species. Measurements and modeling studies (see e.g., [68] and references therein) indicate that at 70–80 km, corresponding to the reference height used here, the effective recombination coefficient generally lies near 10^{-11} $m^3 s^{-1}$ during the flare-induced ionization enhancements. Thus, the value derived for this event agrees well with the theoretical expectations and previous observational results.

The X1.59 solar flare on 3 July 2021, the first X-class flare of Solar Cycle 25, produced a rare geomagnetic crochet, an almost instantaneous and localized disturbance in Earth's

magnetic field during the flare's peak. We present the first VLF-based analysis of this event, highlighting the rapid response of the lower ionosphere to solar-flare radiation. Strong correlations were observed between X-ray flux peaks and sudden changes in VLF signal amplitude and phase, with amplitude increases consistent with flare intensity and unusually large phase variations likely influenced by the geomagnetic crochet. A short ionospheric response delay (60 s) was measured, possibly due to the crochet effect. Importantly, the study focuses on identifying the consequences of the geomagnetic crochet phenomenon on the ionosphere, rather than the ionospheric influence on the crochet itself. The event demonstrates a rapid Sun–Earth coupling mechanism linking flare radiation, ionospheric current enhancement, and detectable VLF disturbances.

3.2. Solar Wind Data

To establish the nature of the SEP enhancement and its potential connection to the July 2021 solar flare, we should eliminate other potential sources. In addition to the absence of CME/ICME events in the databases referred to in Section 2, the main heliospheric parameters that can indicate the class of SEP enhancement were examined. As suggested by the plots in Figure 7, there are no clear or distinctive perturbations of the selected heliospheric parameters, which indicates that a gradual SEP event (typically associated with CME-driven shocks) is unlikely.

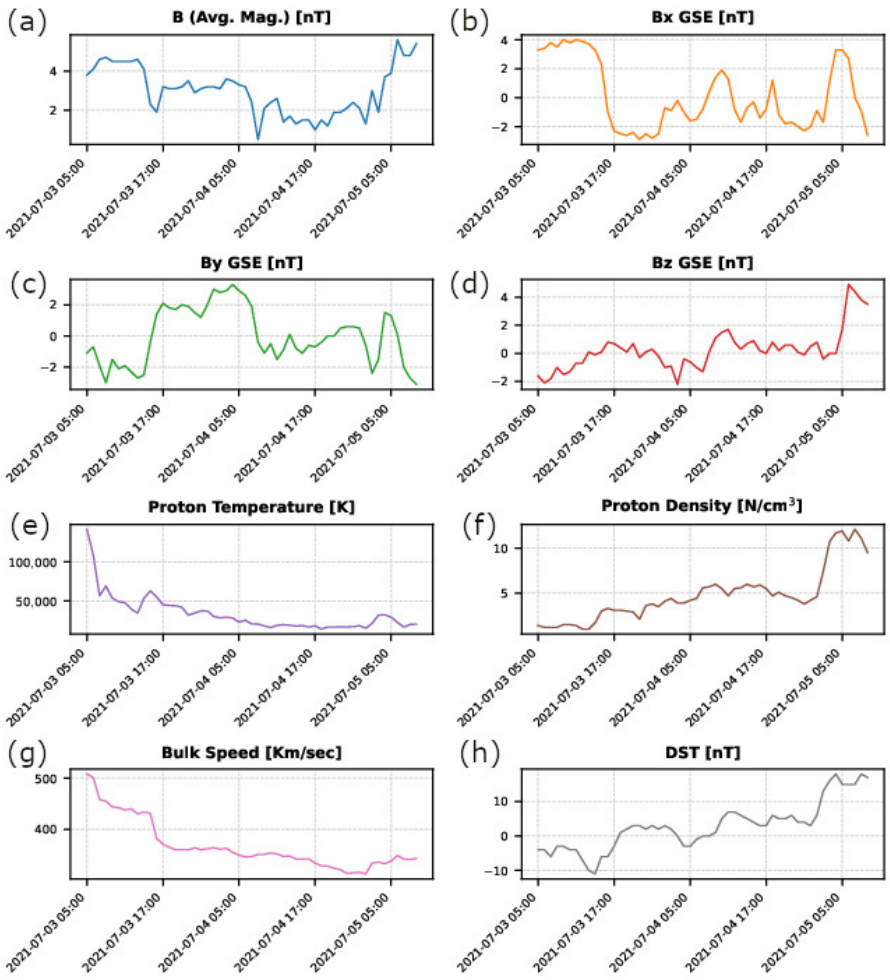

Figure 7. Parameters of the solar wind time series of several heliospheric parameters: IMF, both the total magnitude B (**a**) and its components Bx, By, and Bz ((**b**), (**c**), and (**d**), respectively), proton temperature (**e**), flux density (**f**), solar wind velocity (**g**), and geomagnetic equatorial Dst index (**h**).

Finding energy spectra of proton populations in the 1–100 MeV energy range, measured in situ, presents a challenging problem [74,75] that can be addressed using various possible methods. To calculate the event-integrated flux (or differential fluence), we first defined a time interval for integration. In the absence of external markers (such as perturbation onsets evident in the heliospheric data used for gradual events), this interval was determined based on the timing of the solar flare and the evolution of the spectra, which indicate the duration of the SEP enhancement. The selected interval and the integrated area for the SOHO/ERNE energy channels are illustrated in Figure 8. The baseline for the integration was taken as the mean proton flux after the event had returned to near-background levels.

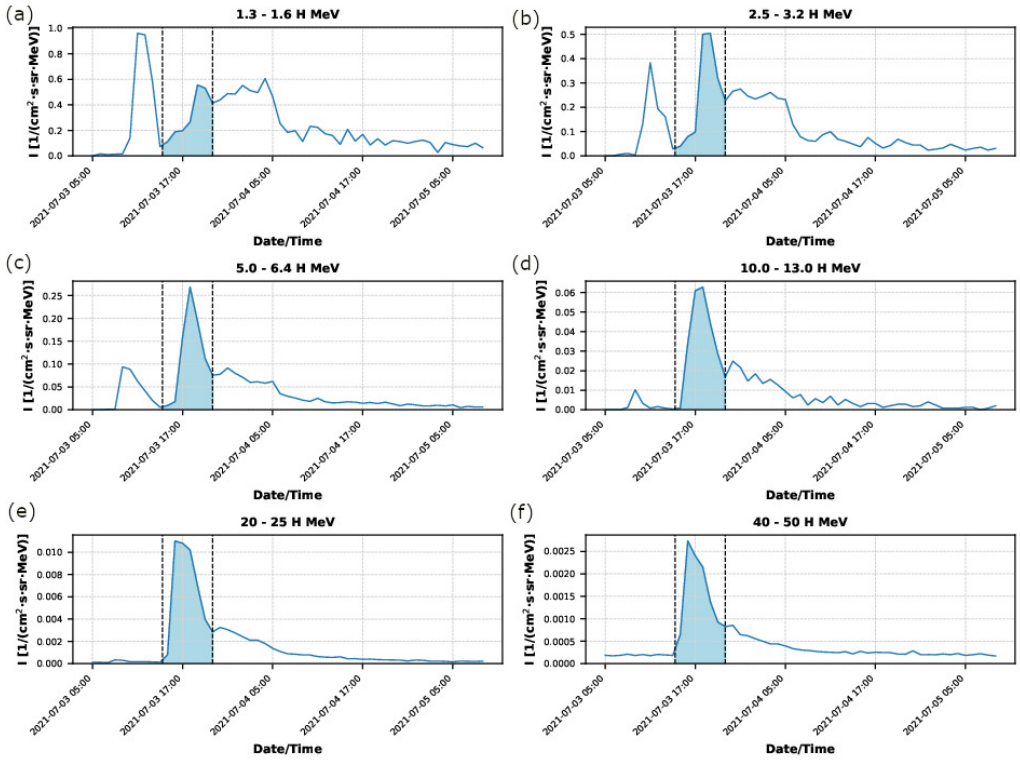

Figure 8. Time series of flux of energetic protons for six selected channels, three LED channels (1.3–1.6 MeV (**a**); 2.5–3.2 MeV (**b**); and 5.0–6.4 MeV (**c**)) and three HED channels (10.0–13.0 MeV (**d**); 20–25 MeV (**e**); and 40–50 MeV (**f**)) measured by the SOHO/ERNE instrument. Vertical dashed lines indicate the time intervals associated with the July 2021 event.

The increase in proton flux at L1 before the time interval associated with the SF is consistent with a relatively small disturbance in the heliosphere, that may be connected to solar activity prior to the SF. It also demonstrates a steady reduction in the relative increase of differential fluence depending on the energy of protons.

To further assess whether the enhancement can be associated with particles accelerated by the solar-flare-related mechanism, we examined the arrival times of particles at different energies, as illustrated in Figure 9. To determine the arrival time of particles, the half-maximum value of the onset stage was used. First, it was necessary to determine the onset time, which was defined as the first time the derivative of the smoothed intensity exceeded a threshold (proportional to the noise level) and the intensity rose above twice the background median absolute deviation (MAD). The peak time was taken as the time of maximum intensity, and the half-maximum time as the first point where the intensity exceeded the halfway value between baseline and peak. Background noise in each energy channel was estimated using the above mentioned MAD, scaled to match the standard

deviation for Gaussian noise. This provides a stable estimate of fluctuations in the baseline preceding the event while being insensitive to outliers. To quantify the timing uncertainty at half-maximum, the local slope of the intensity rise was measured by fitting a straight line to a small window (± 2 points) of the smoothed time series centered on the half-max crossing. The timing uncertainty, σ_t, was then estimated as:

$$\sigma_t \approx \sigma / |dF/dt|, \tag{1}$$

where σ is the MAD-based background noise and dF/dt is the fitted slope. To account for the finite time resolution, a cadence floor equal to half the measurement interval was enforced, ensuring a minimum uncertainty for very fast rises or low-noise channels.

A relative timing uncertainty was also computed:

$$\sigma_{t_{Relative}} = \sigma_t / (t_{halfmax} - t_{onset}), \tag{2}$$

where $t_{halfmax}$ is the time corresponding to half of the maximum, n and the onset stage and t_{onset} is the time corresponding to the beginning of the onset phase. To be accepted for the analysis, each point had to pass a quality check that removed points where the determination of onset, maximum, or half-maximum failed or produced extreme values, where the slope was poorly defined, or where the relative uncertainty had an unreasonable value. The half-max times of all channels are plotted against energy (or inverse velocity) as shown in Figure 9. Channels flagged as good are shown in green, while bad or uncertain channels are plotted in dark red. This allows quick assessment of which channels provide reliable timing information while keeping the plots uncluttered, without plotting the sometimes overlapping timing error bars. Clear velocity dispersion is observed, with higher-energy particles arriving earlier and lower-energy channels showing delayed onsets relative to the high-energy channels. This behavior is consistent with the assumption that the detected particles are of solar origin.

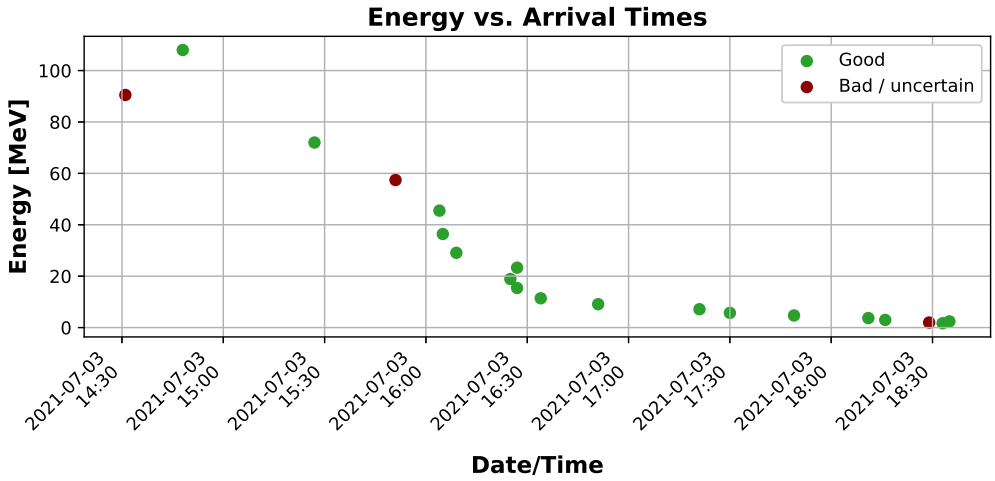

Figure 9. Arrival times of the recorded half-of-max value of the proton flux in different energy bins. Channels flagged as good based on the procedure explained in text are shown in green, while uncertain channels are plotted in dark red.

The differential energetic proton flux in each energy channel, integrated over the duration of the event, is used to construct the differential fluence spectrum, serving as the final step in characterizing the SEP event. Several models have been proposed to describe differential fluence spectra of various particle species [76]. Among these, the model proposed by Ellison and Ramaty, developed on the basis of observations of particle acceleration

at interplanetary shocks [77], reasonably successfully reproduces the characteristic spectral shape often observed in extreme events [78,79]. This model assumes a power-law form with an exponential rollover to describe the energetic particle fluence spectrum:

$$\frac{dJ}{dE} = AE^{\gamma} \exp\left(-\frac{E}{E_0}\right), \tag{3}$$

where E is the particle energy, E_0 is the cutoff exponent parameter, γ is the spectral index, and A is the spectral coefficient. Even though there are newer proposed models, we found the Ellison–Ramaty model to be mostly in good agreement with the observed SOHO/ERNE data and also robust in terms of the convergence of the fit.

The observed differential integral flux is several orders of magnitude lower than typically recorded during gradual SEP events associated with CMEs [80]. This proton flux reflects the prevailing heliospheric conditions during the event, which include a relatively weak interplanetary magnetic field configuration and limited shock acceleration efficiency in the inner heliosphere. Consequently, proton transport and acceleration within the heliosphere were less effective, leading to suppressed low-energy proton intensities compared to large, CME-dominated SEP events. The shape of the energetic proton fluence spectra during the July 2021 event is shown in Figure 10, where the average channel energy in MeV was used for particle energy bin values [81]. The spectra are reasonably well modeled by the Ellison–Ramaty function in the higher-energy channels, while agreement is poor for the lowest-energy channels. Both observations, regarding the flux magnitude and the spectral shape, are consistent with the July solar flare as the assumed source of the enhancement. It should be noted, however, that the total magnitude of the enhancement remains insufficient to classify it officially as a SEP event, and as a result it does not appear in online SEP event repositories.

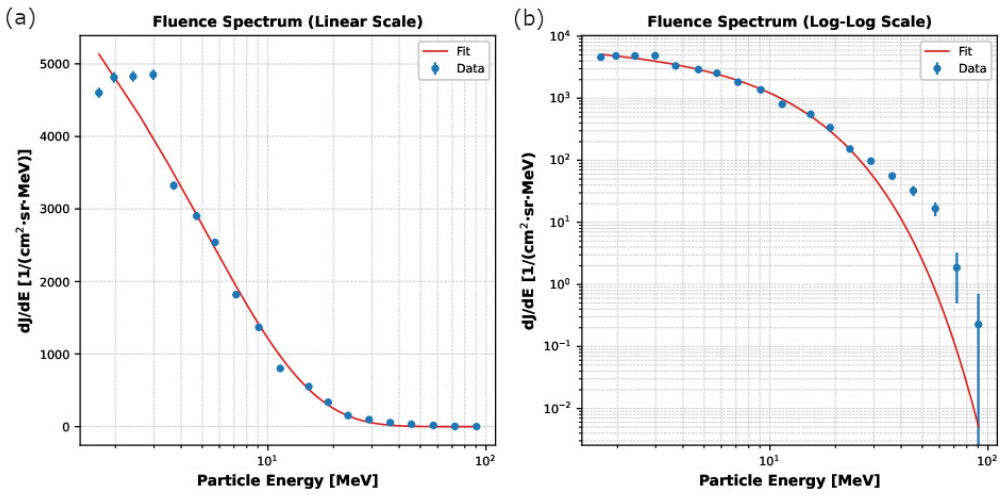

Figure 10. SEP fluence spectrum during the July 2021 event in linear (**a**) and log-log (**b**) scale. The red line represents the Ellison-Ramaty fit of the differential integral flux of each bin represented with blue dots.

3.3. Cosmic Rays

The X1.59 solar flare of 3 July 2021 produced only minimal effects on galactic cosmic rays (GCRs), with no statistically significant Forbush decrease observed. Although the event was accompanied by a modest enhancement of solar energetic particles detected by GOES-16, the associated proton flux remained weak and did not reach ground-level enhancement (GLE) energies. This limited response is attributed to the flare's location near the solar limb and the properties of the associated coronal mass ejection (CME),

which was relatively weak and only partially Earth-directed, resulting in poor magnetic connectivity with near-Earth space. Consequently, the interplanetary disturbance lacked the strength and favorable orientation required to suppress the GCR flux at the Earth. Neutron monitor observations [82], including those from low cut-off rigidity stations like Oulu and the South Pole station, exhibited only minor background fluctuations rather than the characteristic intensity decrease associated with a Forbush event (Figure 11). Overall, cosmic-ray modulation during this event was negligible, reflecting the limited geoeffectiveness of the heliospheric structures produced by the flare and its CME.

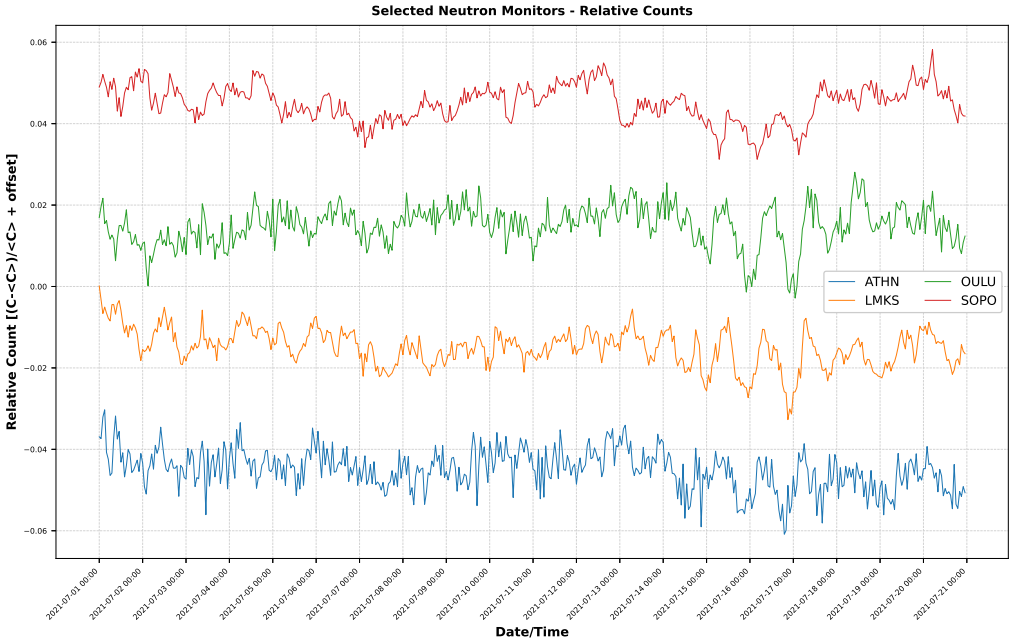

Figure 11. Hourly time series of ground level CR intensities recorded by selected neutron monitor stations of the global network during July 2021: Athens (ATHN), Lomnický Štít (LMKS), Oulu (OULU), and South Pole (SOPO).

4. Conclusions and Perspectives

The X1.59 solar flare on 3 July 2021, the first X-class flare of Solar Cycle 25, produced a rare geomagnetic crochet and strong ionospheric responses. To the best of our knowledge, this study represents the first VLF-based analysis of this event, as well as the first comprehensive multi-instrument investigation of it. This study highlights the importance of ionospheric responses by applying a multi-instrument analysis to provide a comprehensive Sun–Earth overview of the events. VLF observations of NAA and DHO signals at the IPB, combined with modeling, revealed rapid changes in effective reflection height h', sharpness β, time delay and electron density profiles. Cosmic-ray measurements showed negligible modulation, with no significant Forbush decrease, reflecting the flare's weak and partially Earth-directed CME. These results demonstrate the sensitivity of the lower ionosphere to sudden solar radiation enhancements and highlight the effectiveness of combining VLF monitoring, modeling, and cosmic-ray observations to assess flare-driven space-weather effects.

Future work should integrate various measurements with VLF measurements, GNSS data, neutron and muon monitors, and spaceborne X-ray/EUV observations to provide a more complete Sun-to-Earth picture of flare and CME impacts. Improving ionospheric modeling and applying machine-learning methods will enhance the accuracy of parameters during rapid disturbances. As Solar Cycle 25 intensifies, coordinated studies of cosmic-ray

modulation and ionospheric response will refine space-weather forecasting and support more resilient communication and navigation systems.

Recent advances, such as real-time ionospheric data assimilation, physics-informed inverse reconstruction, and machine-learning frameworks incorporating supervised and hybrid training, substantially improve model skill during extreme disturbances. In this context, the X1.59 solar flare of 3 July 2021 provides a valuable event-specific dataset, and derived parameters that can be used as benchmark inputs, feature vectors, and validation targets for next-generation space-weather prediction systems.

Author Contributions: Conceptualization, V.A.S.; writing—original draft preparation, V.A.S. and N.V.; writing—review and editing, V.A.S., N.V., A.K., M.S., Ž.M., F.A. and M.L. The authors had full access to the data and took responsibility for their integrity. All authors have read and agreed to the published version of the manuscript.

Funding: Funding for this study was provided by the Institute of Physics Belgrade, University of Belgrade, through the Ministry of Science, Technological Development and Innovations of the Republic of Serbia.

Institutional Review Board Statement: Not applicable.

Informed Consent Statement: Not applicable.

Data Availability Statement: The data presented in this study are available on request from the corresponding author. The data are not publicly available due to privacy.

Acknowledgments: We would like to express our gratitude to the reviewers for constructive comments and useful suggestions that significantly contributed to the quality of the manuscript. The article is based upon work from COST Action CA24101—FuSe, supported by COST (European Cooperation in Science and Technology). OMNI data was made available by NASA/GSFC's Space Physics Data Facility's OMNIWeb service. This CME catalog is generated and maintained at the CDAW Data Center by NASA and The Catholic University of America in cooperation with the Naval Research Laboratory. SOHO is a project of international cooperation between ESA and NASA. We acknowledge the NMDB database, founded under the European Union's FP7 program (contract No. 213007) for providing data.

Conflicts of Interest: The authors declare no conflict of interest.

References

1. Waterfall, C.O.G.; Dalla, S.; Raukunen, O.; Heynderickx, D.; Jiggens, P.; Vainio, R. High Energy Solar Particle Events and Their Relationship to Associated Flare, CME and GLE Parameters. *Space Weather* **2023**, *21*, e2022SW003334. [CrossRef]
2. Tsurutani, B.T.; Gonzalez, W.D. The Interplanetary causes of magnetic storms: A review *J. Geophys. Res.* **1997**, *98*, 77–89. [CrossRef]
3. Hargreaves, J.K. *The Solar-Terrestrial Environment*; Cambridge University Press: Cambridge, UK, 1992.
4. Lanzerotti, L.J. Space Weather Effects on Communications. In *Proceedings of the Space Storms and Space Weather Hazards*; Daglis, I.A., Ed.; Springer: Berlin/Heidelberg, Germany, 2001, p. 313.
5. Cid, C.; Palacios, J.; Saiz, E.; Guerrero, A.; Cerrato, Y. On extreme geomagnetic storms. *J. Space Weather Space Clim.* **2014**, *4*, A28. [CrossRef]
6. Miteva, R.; Samwel, S.W.; Tkatchova, S. Space Weather Effects on Satellites. *Astronomy* **2023**, *2*, 165–179. [CrossRef]
7. Ishii, M.; Berdermann, J.; Forte, B.; Hapgood, M.; Bisi, M.M.; Romano, V. Space weather impact on radio communication and navigation. *Adv. Space Res.* **2024**. [CrossRef]
8. McRae, W.M.; Thomson, N.R. Solar flare induced ionospheric D-region enhancements from VLF phase and amplitude observations. *J. Atmos. Sol.-Terr. Phys.* **2004**, *66*, 77–87. [CrossRef]
9. Thomson, N. Experimental daytime VLF ionospheric parameters. *J. Atmos. Terr. Phys.* **1993**, *55*, 173–184. [CrossRef]
10. Thomson, N.R.; Rodger, C.J.; Clilverd, M.A. Daytime D region parameters from long-path VLF phase and amplitude. *J. Geophys. Res. Space Phys.* **2011**, *116*, *A11*. [CrossRef]
11. Pandey, U.; Singh, B.; Singh, O.P.; Saraswat, V.K. Solar flare induced ionospheric D-region perturbation as observed at a low latitude station Agra, India. *Astrophys. Space Sci.* **2015**, *357*, 35. [CrossRef]
12. Sripathi, S.; Balachandran, N.; Veenadhari, B.; Singh, R.; Emperumal, K. Response of the equatorial and low-latitude ionosphere to an intense X-class solar flare (X7/2B) as observed on 09 August 2011. *J. Geophys. Res. Space Phys.* **2013**, *118*, 2648–2659. [CrossRef]

13. Grubor, D.; Šulić, D.; Žigman, V. Classification of X-ray solar flares regarding their effects on the lower ionosphere electron density profile. *Ann. Geophys.* **2008**, *26*, 1731–1740. [CrossRef]
14. Bekker, S. Assessment of Vertical Redistribution of Electron Density in Ionosphere During an X-Class Solar Flare Using GNSS Data. *Atmosphere* **2025**, *16*, 825. [CrossRef]
15. Wait, J.R.; Spies, K.P. *Characteristics of the Earth–Ionosphere Waveguide for VLF Radio Waves*; Technical Report Technical Note 300; National Bureau of Standards: Gaithersburg, MD, USA, 1964.
16. Kelley, M.C. *The Earth's Ionosphere: Plasma Physics and Electrodynamics*, 2nd ed.; Academic Press: Cambridge, MA, USA, 2009.
17. Grubor, D.; Šulić D..; Žigman, V. Influence of Solar X-ray Flares on the Earth-Ionosphere Waveguide. *Serbian Astron. J.* **2005**, *171*, 29–35. [CrossRef]
18. Thomson, N.R.; Clilverd, M.A.; Rodger, C.J. Midlatitude ionospheric D region: Height, sharpness, and solar zenith angle. *J. Geophys. Res.* **2017**, *122*, 8933–8946. [CrossRef]
19. Thomson, N.R.; Clilverd, M.A.; Rodger, C.J. Ionospheric D Region: VLF-Measured Electron Densities Compared With Rocket-Based FIRI-2018 Model. *J. Geophys. Res.* **2022**, *127*, e2022JA030977. [CrossRef]
20. Srećković, V.A.; Dimitrijević, M.S.; Mijić, Z.R. Data in Astrophysics and Geophysics: Novel Research and Applications. *Data* **2024**, *9*, 32. [CrossRef]
21. Thomson, N.R.; Clilverd, M.A.; Rodger, C.J. Ionospheric D Region: Characteristics Near Dawn and Dusk. *J. Geophys. Res.* **2025**, *130*, e2024JA033610. [CrossRef]
22. Raulin, J.P.; Abe Pacini, A.; Kaufmann, P.; Correia, E.; Aparecida G. Martinez, M. On the detectability of solar X-ray flares using very low frequency sudden phase anomalies. *J. Atmos. Sol.-Terr. Phys.* **2006**, *68*, 1029–1035. [CrossRef]
23. Todoroki, Y.; Maekawa, S.; Yamauchi, T.; Horie, T.; Hayakawa, M. Solar flare induced D region perturbation in the ionosphere, as revealed from a short-distance VLF propagation path. *Geophys. Res. Lett.* **2007**, *34*, L03103. [CrossRef]
24. Kumar, A.; Kumar, S. Solar flare effects on D-region ionosphere using VLF measurements during low- and high-solar activity phases of solar cycle 24. *Earth Planets Space* **2018**, *70*, 29. [CrossRef]
25. Rastogi, R.G.; Kaushika, N.D.; Trivedi, N.B. Solar flare crochet and sudden commencement in H within the equatorial electrojet region. *J. Atmos. Terr. Phys.* **1965**, *27*, 663–668. [CrossRef]
26. Broumandan, A.; Tremblay, I.; Kennedy, S. Impact of Solar Cycle 25 on GNSS Measurements: Analysis of Ionospheric Scintillation and Positioning Challenges. *Eng. Proc.* **2025**, *88*, 21. [CrossRef]
27. Tsurutani, B.T.; Verkhoglyadova, O.P.; Mannucci, A.J.; Lakhina, G.S.; Li, G.; Zank, G.P. A brief review of "solar flare effects" on the ionosphere. *Radio Sci.* **2009**, *44*, RS0A17. [CrossRef]
28. Huang, L.; Qi, Z.; Shi, S.; Chen, Y.; Zhao, F.; Wang, X.; Zhu, F.; Li, X.; Feng, P. Study on the Impact of C-Class Solar Flares on Low-Frequency Signal Propagation and Ionospheric Disturbances. *Atmosphere* **2025**, *16*, 154. [CrossRef]
29. Yashiro, S.; Gopalswamy, N. Statistical relationship between solar flares and CMEs. *Proc. IAU Symp.* **2009**, *257*, 233–243. [CrossRef]
30. Richardson, I.G.; Cane, H.V. Near-Earth interplanetary coronal mass ejections and their geomagnetic effects. *Sol. Phys.* **2010**, *264*, 189–237. [CrossRef]
31. Forbush, S.E. On the Effects in Cosmic-Ray Intensity Observed During the Recent Magnetic Storm. *Phys. Rev.* **1937**, *51*, 1108–1109. [CrossRef]
32. Cane, H.V. Coronal Mass Ejections and Forbush Decreases. *Space Sci. Rev.* **2000**, *93*, 55–77. [CrossRef]
33. Ahluwalia, H.S. Solar Wind Modulation of Galactic Cosmic Rays. In *AGU Fall Meeting Abstracts, Proceedings of the AGU Fall Meeting Abstracts, San Francisco, CA, USA, 6–10 December 2002*; SH11A–0377; AGU: Washington, DC, USA, 2022.
34. Belov, A.; Shlyk, N.; Abunina, M.; Belova, E.; Abunin, A.; Papaioannou, A. Solar Energetic Particle Events and Forbush Decreases Driven by the Same Solar Sources. *Universe* **2022**, *8*, 403. [CrossRef]
35. Riley, P. On the probability of occurrence of extreme space weather events. *Space Weather* **2012**, *10*, S02012. [CrossRef]
36. Srećković, V.A. New Challenges in Exploring Solar Radiation: Influence, Consequences, Diagnostics, Prediction. *Appl. Sci.* **2023**, *13*, 4126. [CrossRef]
37. Eastwood, J.; Biffis, E.; Hapgood, M.; Green, L.; Bisi, M.; Bentley, R.; Wicks, R.; McKinnell, L.A.; Gibbs, M.; Burnett, C. The economic impact of space weather: Where do we stand? *Risk Anal.* **2017**, *37*, 206–218. [CrossRef]
38. Zolesi, B.; Cander, L. *Ionospheric Prediction and Forecasting*; Springer: Berlin/Heidelberg, Germany, 2014. [CrossRef]
39. Savić, M.; Veselinović, N.; Dragić, A.; Maletić, D.; Joković, D.; Udovičić, V.; Banjanac, R.; Knežević, D. New insights from cross-correlation studies between solar activity indices and cosmic-ray flux during Forbush decrease events. *Adv. Space Res.* **2023**, *71*, 2006–2016. [CrossRef]
40. Curto, J.J.; Gaya-Piqué, L.R. Geoeffectiveness of solar flares in magnetic crochet (sfe) production: II—Dependence on the detection method. *J. Atmos. Sol.-Terr. Phys.* **2009**, *71*, 1705–1710. [CrossRef]
41. Dodson, H.W.; Hedeman, E.R. Crochet-Associated Flares. *Astrophys. J.* **1958**, *128*, 636. [CrossRef]
42. Pintér, Š.. Geomagnetic crochets of solar flares observed in Hurbanovo. *Bull. Astron. Institutes Czechoslov.* **1967**, *18*, 274.

43. Richmond, A.D.; Venkateswaran, S.V. Geomagnetic Crochets and Associated Ionospheric Current Systems. *Radio Sci.* **1971**, *6*, 139–164. [CrossRef]
44. CDAW. Lasco CME Catalog and Major SEP Event List. Available online: https://cdaw.gsfc.nasa.gov/ (accessed on 10 November 2025).
45. Reames, D.V. The Two Sources of Solar Energetic Particles. *Space Sci. Rev.* **2013**, *175*, 53–92. [CrossRef]
46. Oljira, A. A study of Solar Flares and Geomagnetic Storms Impact on Total Electron Content Over High-Latitude Region During July- November 2021: The Case of Tromso Station. *Adv. Space Res.* **2023**, *72*, 3868–3881. [CrossRef]
47. Rao, S.S.; Srivastava, N.; Chakraborty, M.; Kumar, S.; Chakrabarty, D. Observations of Geomagnetic Crochet at High-Latitudes Due To X1.5 Class Solar Flare on 3 July 2021. *Space Weather* **2024**, *22*, e2023SW003719. [CrossRef]
48. López-Urias, C.; Vazquez-Becerra, G.E.; Nayak, K.; López-Montes, R. Analysis of Ionospheric Disturbances during X-Class Solar Flares (2021–2022) Using GNSS Data and Wavelet Analysis. *Remote Sens.* **2023**, *15*, 4626. [CrossRef]
49. Fagundes, P.R.; Pillat, V.G.; Tardelli, A.; Muella, M.T.A.H. Pole-to-Pole Ionospheric Disturbances Due to Solar Flares During Low Solar Activity. *J. Geophys. Res. Space Phys.* **2024**, *129*, e2024JA032597. [CrossRef]
50. Srećković, V.A.; Kolarski, A.; Langović, M.; Arnaut, F.; Jevremović, S.; Mijić, Z.R. The strongest solar flares of Solar Cycle 25 and their subionospheric impact: Data and modeling. *Contrib. Astron. Obs. Skaln. Pleso* **2025**, *55*, 88–94. [CrossRef]
51. Spaceweather.com. X1.5-class Solar Flare and Radio Blackout. 3 July 2021. Available online: https://www.spaceweather.com (accessed on 12 February 2025).
52. NOAA Space Weather Prediction Center. R3 Strong Radio Blackout Event Summary. 3 July 2021. GOES XRS Event Archive. Available online: https://www.swpc.noaa.gov (accessed on 12 February 2025).
53. NASA SDO and NOAA GOES Missions. SDO/AIA Imagery and GOES X-Ray Flux Data for the 3 July 2021 X1.59 Solar Flare. Event Data Set. Available online: https://sdo.gsfc.nasa.gov/ (accessed on 12 February 2025).
54. GSFC NASA. OMNIWeb Plus Service. Available online: https://omniweb.gsfc.nasa.gov/ (accessed on 10 November 2025).
55. Torsti, J.; Valtonen, E.; Lumme, M.; Peltonen, P.; Eronen, T.; Louhola, M.; Riihonen, E.; Schultz, G.; Teittinen, M.; Ahola, K.; et al. Energetic particle experiment ERNE. *Sol. Phys.* **1995**, *162*, 505–531. [CrossRef]
56. Paassilta, M.; Raukunen, O.; Vainio, R.; Valtonen, E.; Papaioannou, A.; Siipola, R.; Riihonen, E.; Dierckxsens, M.; Crosby, N.; Malandraki, O.; et al. Catalogue of 55–80 MeV solar proton events extending through solar cycles 23 and 24. *J. Space Weather Space Clim.* **2017**, *7*, A14. [CrossRef]
57. King, J.H.; Papitashvili, N.E. Solar wind spatial scales in and comparisons of hourly Wind and ACE plasma and magnetic field data. *J. Geophys. Res. Space Phys.* **2005**, *110*, A02104. [CrossRef]
58. Yashiro, S.; Gopalswamy, N.; Michalek, G.; St. Cyr, O.C.; Plunkett, S.P.; Rich, N.B.; Howard, R.A. A catalog of white light coronal mass ejections observed by the SOHO spacecraft. *J. Geophys. Res. Space Phys.* **2004**, *109*, A07105. [CrossRef]
59. Richardson, I.; Cane, H. Near-Earth Interplanetary Coronal Mass Ejections Since January 1996. Available online: https://ui.adsabs.harvard.edu/abs/2024harv.data..124R/abstract (accessed on 10 November 2024).
60. Šulić, D.M.; Srećković, V.A.; Mihajlov, A.A. A study of VLF signals variations associated with the changes of ionization level in the D-region in consequence of solar conditions. *Adv. Space Res.* **2016**, *57*, 1029–1043. [CrossRef]
61. Srećković, V.A.; Šulić, D.M.; Ignjatović, L.; Vujčić, V. Low Ionosphere under Influence of Strong Solar Radiation: Diagnostics and Modeling. *Appl. Sci.* **2021**, *11*, 7194. [CrossRef]
62. Šulić, D.M.; Srećković, V.A. A Comparative Study of Measured Amplitude and Phase Perturbations of VLF and LF Radio Signals Induced by Solar Flares. *Serbian Astron. J.* **2014**, *188*, 45–54. [CrossRef]
63. Nina, A.; Simić, S.; Srećković, V.A.; Popović, L.Č. Detection of short-term response of the low ionosphere on gamma ray bursts. *Geophys. Res. Lett.* **2015**, *42*, 8250–8261. [CrossRef]
64. Srećković, V.A.; Šulić, D.M.; Vujčić, V.; Jevremović, D.; Vyklyuk, Y. The effects of solar activity: Electrons in the terrestrial lower ionosphere. *J. Geogr. Inst. Jovan Cvijic SASA* **2017**, *67*, 221–233. [CrossRef]
65. Kolarski, A.; Srećković, V.A.; Mijić, Z.R. Monitoring solar activity during 23/24 solar cycle minimum through VLF radio signals. *Contrib. Astron. Obs. Skaln. Pleso* **2022**, *52*, 105–115. [CrossRef]
66. Kolarski, A.; Veselinović, N.; Srećković, V.A.; Mijić, Z.; Savić, M.; Dragić, A. Impacts of Extreme Space Weather Events on September 6th, 2017 on Ionosphere and Primary Cosmic Rays. *Remote Sens.* **2023**, *15*, 1403. [CrossRef]
67. Nina, A.; Čadež, V.M.; Popović, L.Č.; Srećković, V.A. Diagnostics of plasma in the ionospheric D-region: Detection and study of different ionospheric disturbance types. *Eur. Phys. J. D* **2017**, *71*, 189. [CrossRef]
68. Žigman, V.; Grubor, D.; Šulić, D. D-region electron density evaluated from VLF amplitude time delay during X-ray solar flares. *J. Atmos. Sol.-Terr. Phys.* **2007**, *69*, 775–792. [CrossRef]
69. Žigman, V.; Dominique, M.; Grubor, D.; Rodger, C.J.; Clilverd, M.A. Lower-ionosphere electron density and effective recombination coefficients from multi-instrument space observations and ground VLF measurements during solar flares. *J. Atmos. Sol.-Terr. Phys.* **2023**, *247*, 106074. [CrossRef]
70. Srećković, V.A.; Šulić, D.M.; Vujčić, V.; Mijić, Z.R.; Ignjatović, L.M. Novel Modelling Approach for Obtaining the Parameters of Low Ionosphere under Extreme Radiation in X-Spectral Range. *Appl. Sci.* **2021**, *11*, 11574. [CrossRef]

71. Hayes, L.A.; O'Hara, O.S.D.; Murray, S.A.; Gallagher, P.T. Solar Flare Effects on the Earth's Lower Ionosphere. *Sol. Phys.* **2021**, *296*, 157. [CrossRef]
72. Barta, V.; Natras, R.; Srećković, V.; Koronczay, D.; Schmidt, M.; Šulic, D. Multi-instrumental investigation of the solar flares impact on the ionosphere on 05–06 December 2006. *Front. Environ. Sci.* **2022**, *10*, 904335. [CrossRef]
73. Kolarski, A.; Srećković, V.A.; Mijić, Z.R. Response of the Earth's Lower Ionosphere to Solar Flares and Lightning-Induced Electron Precipitation Events by Analysis of VLF Signals: Similarities and Differences. *Appl. Sci.* **2022**, *12*, 582. [CrossRef]
74. Logachev, Y.; Kecskeméty, K.; Zeldovich, M.A. Energy Spectra of low-Flux Protons in the Inner Heliosphere under Quiet Solar Conditions. *Sol. Phys.* **2002**, *208*, 141–166. [CrossRef]
75. Kecskeméty, K.; Logachev, Y.I.; Zeldovich, M.A.; Kóta, J. Modulation of the Galactic Low-energy Proton Spectrum in the Inner Heliosphere. *Astrophys. J.* **2011**, *738*, 173. [CrossRef]
76. Mottl, D.A.; Nymmik, R.A.; Sladkova, A.I. Energy spectra of high-energy SEP event protons derived from statistical analysis of experimental data on a large set of events. *AIP Conf. Proc.* **2001**, *552*, 1191–1196. [CrossRef]
77. Ellison, D.C.; Ramaty, R. Shock acceleration of electrons and ions in solar flares. *Astrophys. J.* **1985**, *298*, 400–408. [CrossRef]
78. Nymmik, R.A. Inflections (knees) in wide-range spectra of solar energetic protons and heavy ions: Their form, parameters, and regularities. *Bull. Russ. Acad. Sci. Phys.* **2011**, *75*, 761–763. [CrossRef]
79. Miroshnichenko, L.; Nymmik, R. Extreme fluxes in solar energetic particle events: Methodological and physical limitations. *Radiat. Meas.* **2014**, *61*, 6–15. [CrossRef]
80. Savić, M.; Veselinović, N.; Maričić, D.; Šterc, F.; Banjanac, R.; Travar, M.; Dragić, A. Further Study of the Relationship between Transient Effects in Energetic Proton and Cosmic Ray Fluxes Induced by Coronal Mass Ejections. *Universe* **2024**, *10*, 283. [CrossRef]
81. Vainio, R.; Valtonen, E.; Heber, B.; Malandraki, O.E.; Papaioannou, A.; Klein, K.L.; Afanasiev, A.; Agueda, N.; Aurass, H.; Battarbee, M.; et al. The first SEPServer event catalogue 68-MeV solar proton events observed at 1 AU in 1996–2010. *J. Space Weather Space Clim.* **2013**, *3*, A12. [CrossRef]
82. Christian-Albrechts-Universität zu Kiel. NMDB: The Neutron Monitor Database. Available online: https://www.re3data.org/repository/r3d100012328 (accessed on 22 September 2025).